Design and Implementation of a Liquid Nitrogen-Cooled Hollow Cathode Discharge Source for the Study of the Reaction $H_3^+ + H_2 \rightarrow H_2 + H_3^+$ at Physically Relevant Temperatures and the Study of the $B^3\Pi_g \rightarrow A^3\Sigma_u^+$ Band System of N_2

by

Brett Andrew McGuire

Thesis
for the
Degree of Bachelor of Science
in
Chemistry

College of Liberal Arts and Sciences
University of Illinois
Urbana-Champaign, Illinois

2009

Contents

Acknowledgments

First and foremost, there are three individuals who are largely responsible for shaping me into the scientist I am today. I would like to thank Professor Ben McCall for his invaluable guidance and support both scientifically and academically. I would like to thank Professor Susanna Widicus Weaver for sharing her knowledge and experience in science and life both inside and outside the laboratory. Finally, I would like to thank soon to be Dr. Brian Tom for his unending patience, wisdom, and willingness to explain something to me twenty thousand times until I got it through my thick skull. Were it not for the three people, I wouldn't be writing this thesis, much less preparing to move on to a PhD program.

I would also like to thank the entire McCall research group for their help and support throughout my time here. We have an incredibly fun and supportive group of people here! In particular, I would like to thank Brian Brumfield for taking an annoying sophomore undergraduate under his wing at a most frustrating time for everyone on the C_{60} project and showing him the ropes, and also Andrew Mills for consistently providing an honest point of view and his willingness to repeatedly correct my flawed understanding of electronics. I give both a tip of the hat and wag of the finger to both Brian Siller and Kyle Crabtree for getting me hooked on Linux, providing me endless hours of both joy and unfettered rage.

Finally, and most importantly, I want to thank my parents for fostering my interest in science in the first place and providing me with this incredible opportunity! You guys rock!

Introduction

Work in the McCall group is focused on the study of Astrochemistry, an emerging discipline at the intersection of chemistry and astronomy. Our research involves cutting-edge experimental physical chemistry aimed at understanding the spectroscopic properties of astrophysically relevant species and applying that knowledge to the search for these species and the understanding of their chemistry in interstellar environments. In the laboratory, our experiments are designed to provide high-resolution molecular spectra in conditions of temperature simulating those of the environments of interest. This is achieved through the use of a variety of methods including cavity-ring down spectroscopy and supersonic expansions to obtain rotationally cold molecules, greatly reducing the spectral complexity. One such experiment is the search for a rotationally cold, high-resolution spectrum of Buckminsterfullerene (C_{60}) using a Quantum-Cascade Laser operating at 8.5 μm. Our proficiency with cavity-ringdown techniques was refined in the aquisition of high-resolution spectra of N_2^+ and N_2^* in a positive column discharge. This experiment will be discussed later in detail. Also, we are working on the development of SCRIBES (**S**ensitive **C**ooled **R**esolved **I**on **BE**am **S**pectroscopy), an instrument designed for the high-resolution, cavity-ringdown study of molecules in an ion-beam coupled with a time-of-flight mass spectrometer. Finally, we are interested in the properties and reactivities of H_2 and H_3^+ in the interstellar medium, an experiment that will be discussed here in some detail.

Part I

H_3^+ Spectroscopy

1 Introduction

H_3^+ is a key precursor to ion chemistry in the interstellar medium. It has been employed as an astrophysical probe of conditions of temperature and density due to its ubiquity in a variety of environments. The distribution of *ortho-* and *para-* spin modifications of H_3^+ is particularly interesting in this regard. Consequently, it is important to understand the pathways through which changes to the H_3^+ spin distribution can occur. The descriptor "ortho" applies to a molecule where the intrinsic spin of one or more of the nuclei are anti-aligned to the rest; conversely, the spin of all nuclei in "para" molecules are aligned the same. One possible pathway is the $H_3^+ + H_2 \rightarrow H_2 + H_3^+$ reaction, which proceeds by proton hop and proton exchange and is largely governed by the conservation of nuclear spin. Cordonnier et al. studied this reaction at high temperature in a hollow cathode cell [1], but to facilitate the understanding of astronomical observations, we need lower temperature measurements. Previous work in the McCall group had studied the reaction at lower temperatures in a supersonic expansion [2] in which the ortho:para H_3^+ ratio was measured. In order to better understand this reaction at a variety of conditions typical of interstellar environments, a liquid-nitrogen cooled hollow cathode discharge cell was constructed.

In broad strokes, this experiment uses a hollow cathode to generate a pulse of hydrogenic plasma containing H_3^+ from an H_2 source gas at a variety of *p*ara-H_2 enrichments. Both the resulting *para-* and *ortho*-H_3^+ are then spectroscopically probed using light from a mid-IR laser to determine rotational temperatures and transition intensities. These can then be

used to determine, among other properties, a value α, which represents the ratio of the hop and exchange reactions rates mentioned earlier.

2 Hollow Cathode

2.1 Requirements

In order to qualify as a versatile and long-lived spectrometer, the hollow cathode cell needed to conform to a number of specifications. First, it needed to provide an efficient means for cooling with a variety of liquid and gaseous sources which were completely isolated from the reaction environment. Second, it needed to be capable of achieving and maintaining pressures of less than 50 mTorr while under vacuum. Third, it needed to allow for simple integration of one to two sample gases and at least one pressure sensor. Finally, it was necessary to construct the cell such that it could be used for direct absorption or cavity ring-down spectroscopy without any major adjustments to the cell itself.

Preliminary designs were graciously provided by Takayoshi Amano. These plans were scaled down to a size appropriate for the scope of the experiment and modified to conform to the requirements discussed above. The details of the finalized instrument are discussed in Section 2.2.

2.2 Design

As a guide to the reader, an overview diagram of the instrument is shown in Figure 1.

The main body of the cathode consists of a $\sim$1.6 m long, 85 mm outer diameter (OD) thick-walled glass tube. At the time of construction, precision diameter tubing was unavailable, so a tube was selected which best fit the parts it was to be inserted into. A "T" union was blown into the center of this tube, originally incorrectly using 1" OD glass. Instead of

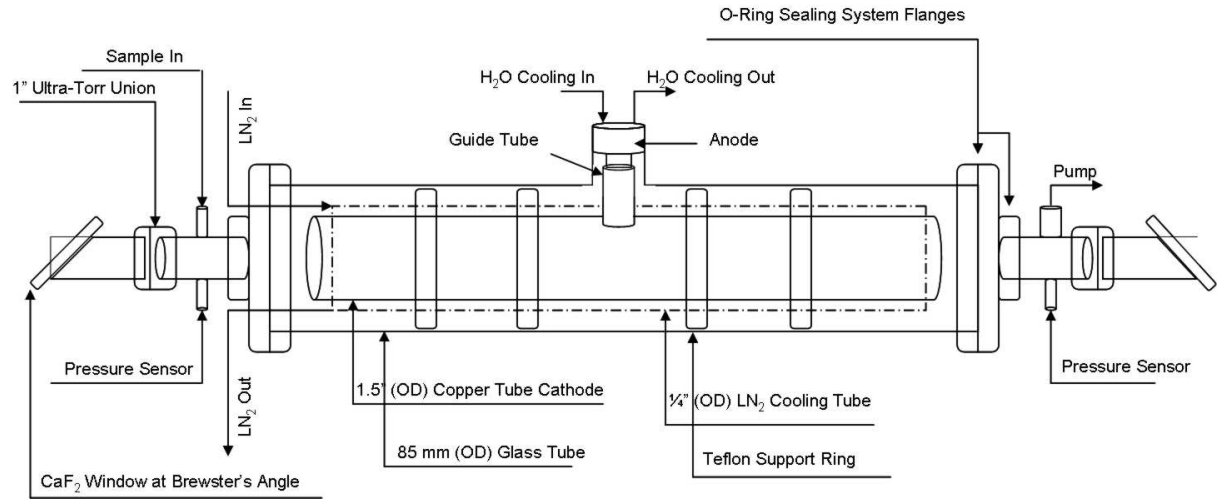

Figure 1: Diagram of major components of the hollow cathode.

commissioning a completely new piece of glass, the correct size glass for the "T" union (1" inner diameter (ID) glass[1]) was blown directly on top of the incorrect tubing and plans for other pieces were adjusted accordingly.

The cathode itself is a 1.4 m long, 1.5" OD copper tube[2] positioned in the center of the glass shell. Around the cathode, 1/4" copper tubing, through which the cooling medium flows, was wrapped tightly and silver-soldered into place. The anode hole, measuring 0.682" in diameter was cut into the side of the cathode at the 0.75 m point, and the cooling lines were wrapped such that significant clearance was left around the hole. The cathode and cooling lines were suspended in the center of the glass shell by means of teflon spacers (Figure 2). These spacers were constructed to an original OD of 3.146" to conform to the experimentally determined ID of the glass shell. The shell itself, however, varied greatly in ID as a function of position, and thus the final OD of the spacers was different for each piece and was determined through trial and error as each was placed into the cell.

The anode (Figure 3) is constructed of stainless-steel and is inserted into the 1" ID tubing at the center of the cell. The vacuum seal is created by two o-rings placed into grooves in the

[1]McMaster-Carr Item # 1176K11
[2]McMaster-Carr Item # 8967K141

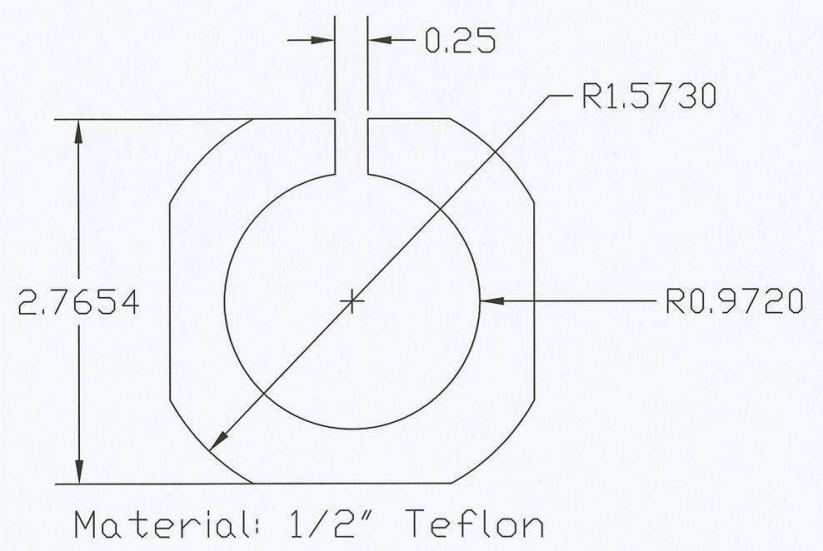

Figure 2: Specifications for teflon spacer rings.

anode itself and sized appropriately to create a seal when inserted into the glass. The bottom tip of the anode was cut at a 45° angle. The body of the anode is hollow and two openings at the top are welded to 1/4" stainless-steel tubing. These tubes protrude approximately 1" from the anode and then bend 90° in opposite directions and continue for approximately 2" before terminating in 1/4" stainless-steel Swagelok connections. These provide an input and output for cooling water that is separate from the cooling lines for the cathode. The discharge is "guided" from the anode to the inside of the cathode by means of a thick-walled quartz tube[3] which slips around the bottom of the anode and fits into the circle cut in the side of the cathode. The bottom of the quartz tube is machine-ground for a snug fit into the cathode.

The ends of the cathode are sealed in a unique way that allows for flexibility in the inputs and optical setups while still maintaining a tight vacuum seal. First, a "face ring" (Figure 4) was constructed from a stock 4 and 5/8" OD Conflat (untapped) blank flange[4]. A 0.9450" clearance hole was cut through the center of the flange. Then, on one side, a circular

[3]Technical Glass Products: 15 mm ID, 18 mm OD Fused Quartz
[4]Kurt J. Lesker Item # F0462X000N

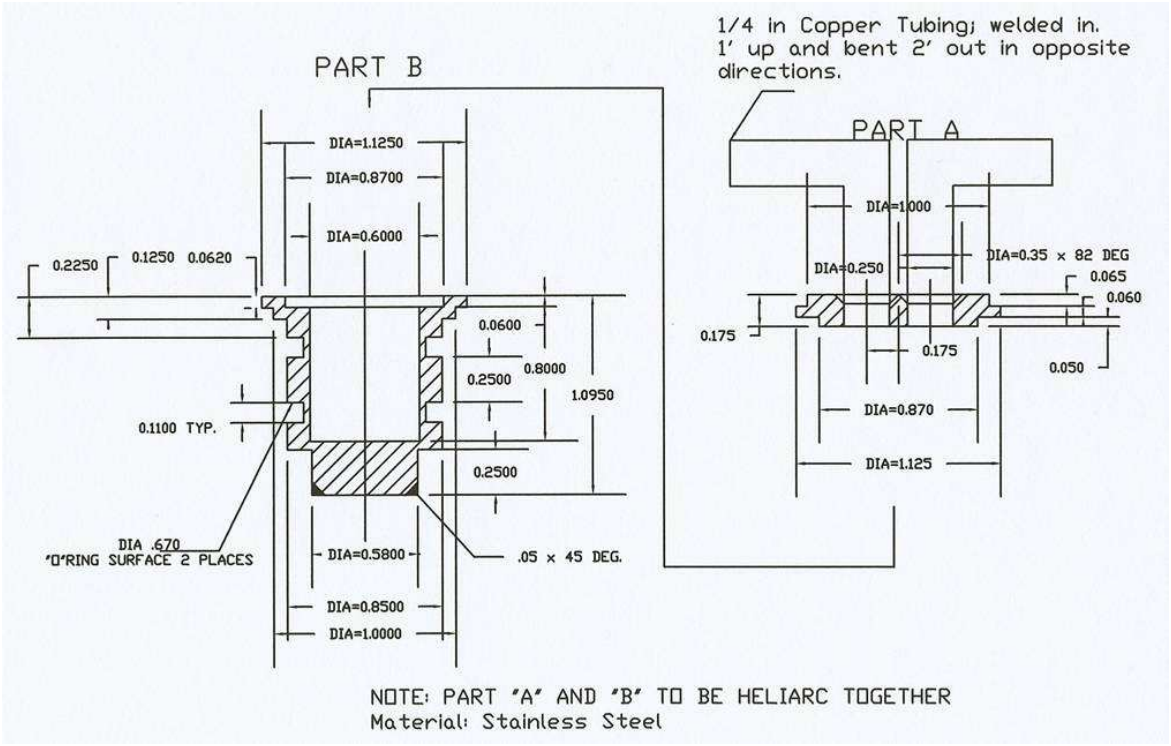

Figure 3: Specifications for the anode.

depression measuring 85 mm in diameter and 0.3125" deep was cut for the glass shell. On the other, a second circular depression measuring 1.0100" in diameter and 0.3125" deep was made to allow the input attachment to slip into. Finally, two through-holes were cut along a radius 1.1020" from the center of the flange and a stainless-steel, 1/4" Swagelok union[5] was welded into each for the cathode cooling lines. Holes were tapped in the flange to allow for the smaller seal ring to attach.

To create the seal to the glass shell, a "seal ring" (Figure 5) was constructed from a stock 4 and 5/8" OD Conflat (tapped) blank flange[6]. A clearance hole was cut straight through the flange at a diameter of 85 mm. This ring was slipped onto the glass shell and an o-ring was placed between it and the face ring. When the face and seal rings were brought together

[5]Swagelok Item # SS-400-1-4W
[6]Kurt J. Lesker Item # F0462X000NT

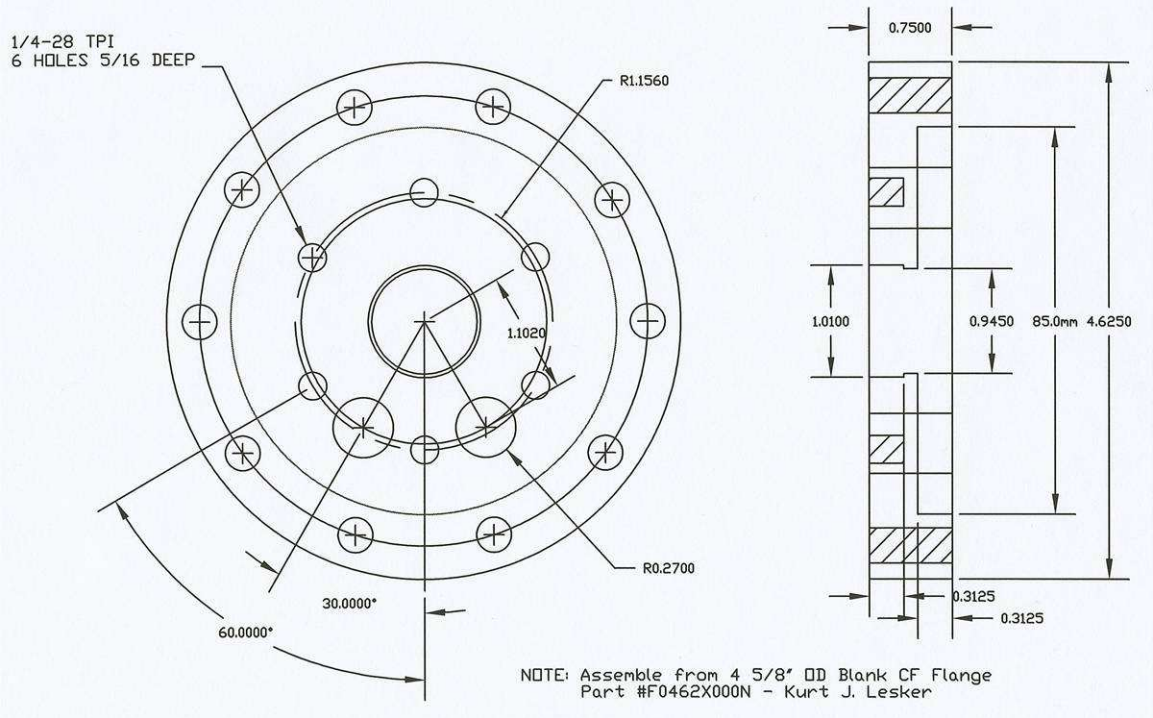

Figure 4: Specifications for the face ring with feedthroughs.

and tightened, the angled groove on the seal ring pushed the o-ring against the face ring and compressed it, forming a tight seal.

To create the seal to the input attachment, a smaller seal ring (Figure 6) was constructed from a stock 2.75" OD Conflat (untapped) blank flange[7]. A feedthrough was cut to allow the input attachment to slide through and rest inside the face ring. An o-ring is placed between this seal ring and the face ring and the seal is formed as before. Additionally, two clearance holes were drilled for the Swagelok feedthroughs for the cooling connections.

The rings at the opposite end of the cell (Figures 7 and 8) where there were no feedthroughs were constructed in a similar fashion but without the feedthrough holes or Swagelok connections. The large seal ring was identical as were the materials used to construct all three rings.

[7]Kurt J. Lesker Item # F0275X000N

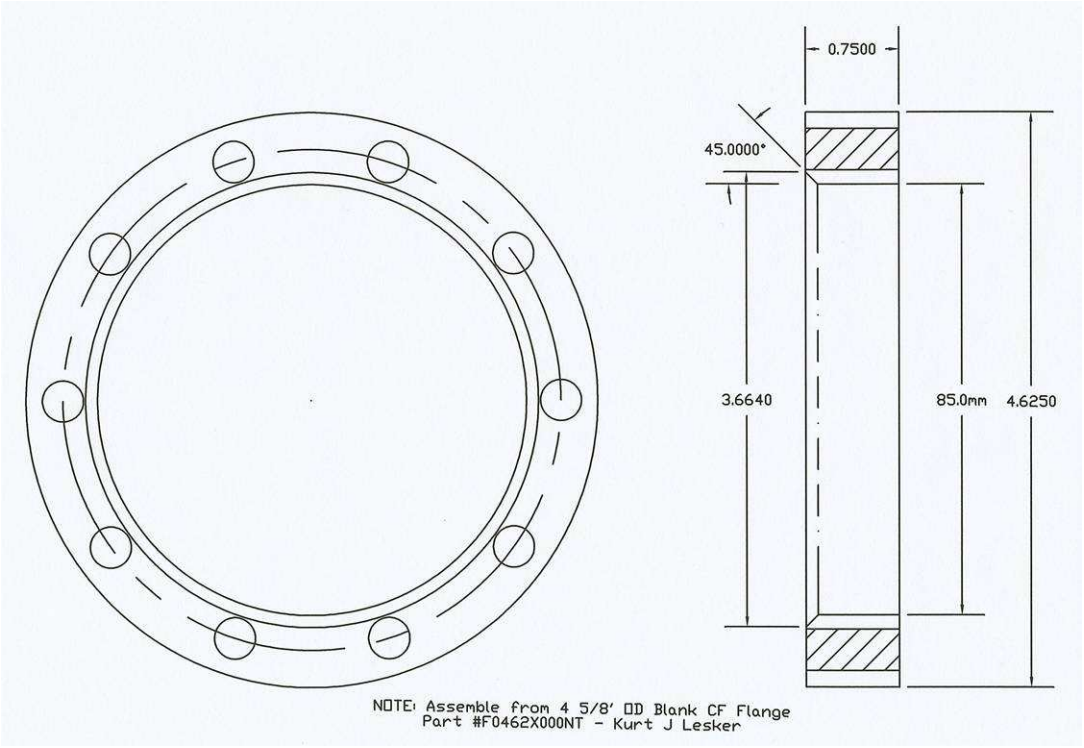

Figure 5: Specifications for the seal ring.

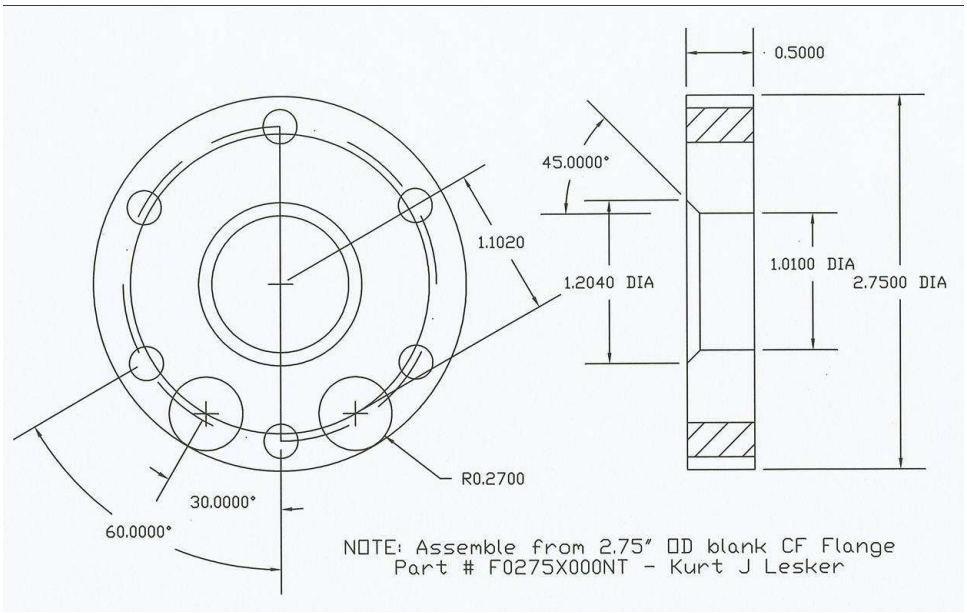

Figure 6: Specifications for the small seal ring with feedthroughs.

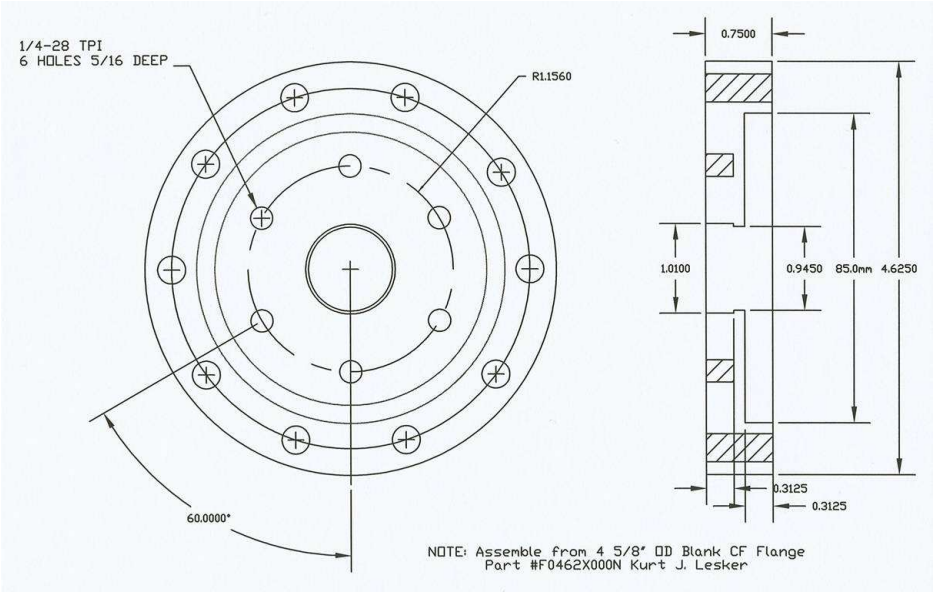

Figure 7: Specifications for the face ring without feedthroughs.

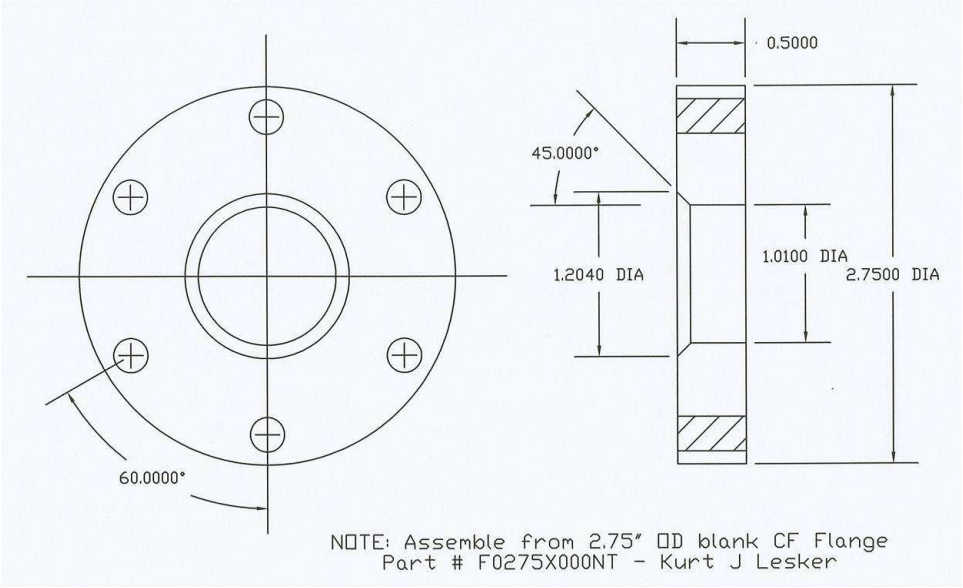

Figure 8: Specifications for the small seal sing without feedthroughs.

The cell is designed so that a variety of input options are available. Any input that can be attached to a 1" OD glass tube can be added to the cell. In its current state, the cell has four inputs: three 1/4" inputs and a 1/2" input (Figure 9). The 1/2" input is currently hooked up to a vacuum pump to allow for the greatest conductance. The remaining 1/4" inputs are divided among two pressure sensors (one at each end) and the input gas.

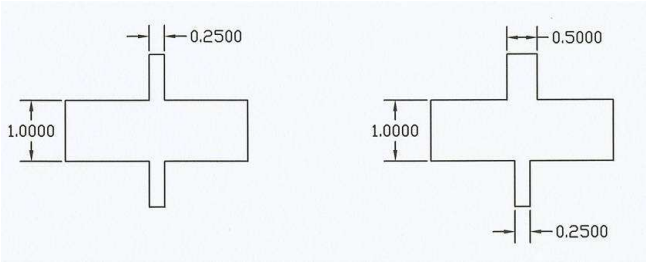

Figure 9: Specifications for the glass inputs.

The glass inputs are designed to be connected to the necessary optical components through a 1" Ultra-torr connection. Currently, these lead to 1" OD, thin-walled stainless-steel tubes, roughly 2.5" long, which are cut at Brewster's angle (55.4°) on the far end. The tubes are sealed with 1.5" diameter, 3 mm thick BaF_2 windows attached with epoxy which are optically transparent at the desired IR wavelengths. This attachment can be modified to provide for virtually any combination of angles and window material, as well as providing a location to mount cavity ring-down mirrors if desired.

2.3 Experimental Setup

The laser beam was generated on another optics table using a nonlinear difference frequency setup. A titanium-sapphire (Ti:Sapph) laser near 824 nm and a neodymium YAG (Nd:YAG) laser at 1064 nm were made collinear and sent through a periodically poled lithium-niobate (PPLN) crystal. Inside the crystal, non-linear processes combined the beams to generate light at the difference of the two laser frequencies. The Nd:YAG is approximately a single-

frequency laser, while the Ti:Sapph is tunable and used to adjust the frequency of the light emerging from the crystal.

This light was then sent to a second optics table containing the hollow cathode and white cell. The beam follows a long path over which it could be made collinear with a beam from a helium-neon laser (HeNe) for alignment purposes. The beam then passed through the White Cell and hollow cathode and was detected by a DC indium-antimonide (InSb) detector.

3 Hollow Cathode Operation and Data Collection

3.1 Experimental Parameters

The sample source for the experiment was *para*-H_2 at a variety of enrichment levels up to 99.99% pure *para*-H_2. The hydrogen was prepared in a helium cryostat converter [5] and the flow rate adjusted to maintain the desired pressure using a hydrogen regulator and a simple needle valve. The background pressure in the cell was typically 10-20 mTorr; the H_2 pressure was kept around 1.850±0.05 Torr throughout the experiment.

The H_3^+ was formed in a plasma discharge inside the hollow cathode cell by a 200 μs, 1 kV pulse. The voltage was generated using a high-voltage power supply which fed a custom-built pulser box. The box contained ballast resistance appropriate for the conditions of the experiment and accepted input from a delay generator. The delay generator triggered the box once every 5 seconds throughout the experiment, giving ample time for the reactants and products from the previous discharge to be removed by the vacuum pump. The box was connected to the anode of the discharge cell using shielded wire and an alligator clip; it was grounded to the cathode.

The absorption signal was detected using a DC InSb detector. Intensity normalization was achieved dividing the absorption peak intensity by the baseline intensity For each run, an average of 10 samples were collected and averaged to generate a single scan.

The R(1,0) transition of *ortho*-H_3^+, R(1,1)^u transition of *para*-H_3^+, and R(2,2)^l transition of *para*-H_3^+ were studied at 2725.898, 2726.219, and 2762.070 cm^{-1}, respectively. These were studied using both water and liquid-nitrogen as a cooling source. A thorough discussion of the results of this experiment, and their implications to our understanding of astronomical processes is described in the thesis of Brian A. Tom and in reference [6].

3.2 White Cell

The laser was aligned using a White Cell multipass configuration for the H_3^+ study. A general sketch of the system is provided (Figure 10).

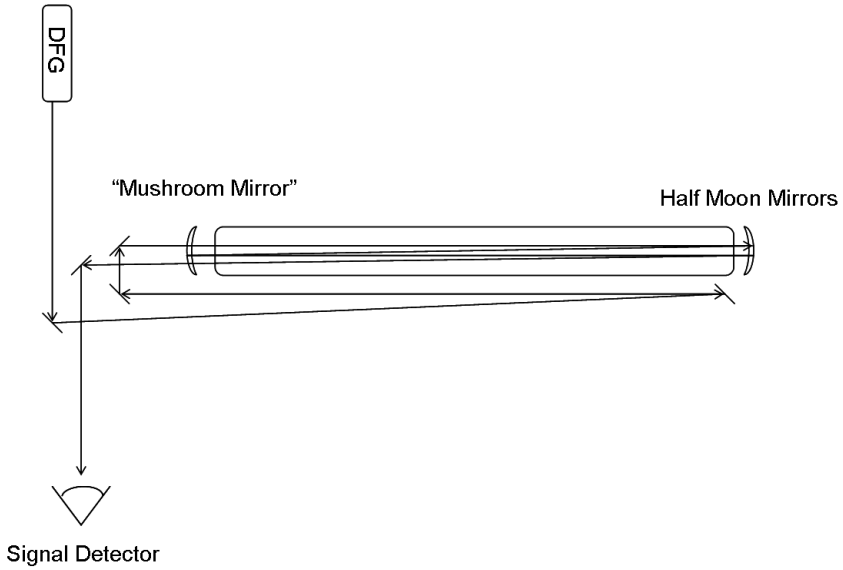

Figure 10: Sketch of the main beam path of the spectrometer

This configuration was first described by John White in 1942 [3]. An illustration of the original White Cell design from White's paper is provided (Figure 11). Three mirrors are needed, all with identical radii of curvature. A White Cell operates by allowing a beam to enter the cell through a slit or other opening at one edge of a mirror (labeled B in Figure 11). The light is imaged on another mirror (labeled A in Figure 11) set a distance away from mirror B equal to exactly the radius of curvature of the mirrors. This light is refocused and

imaged on the far edge of mirror B. Mirror B is then aligned such that the light is focused onto the third mirror (labeled A' in Figure 11), also at a distance away from B equal to the radius of curvature of the mirrors. The light hitting A' is refocused and then imaged on the side of mirror B nearest to the entrance slit. When aligned properly, this results in many successive passes back and forth between mirror B and mirrors A and A', with each successive image on mirror B moving across the mirror horizontally. Eventually, the final image will fall off the edge of mirror B and exit the cell. Aside from the obvious increase in pathlength, this type of cell has the added benefit of re-focusing the image with each reflection, thus significantly reducing the beam divergence which would otherwise occur over such great distances.

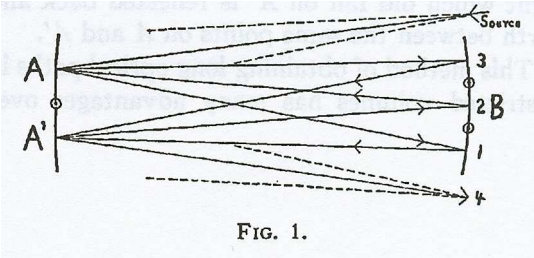

FIG. 1.

Figure 11: Illustration of beam path in multipass White Cell [3]

In this experiment, mirror B was a "mushroom" shaped, 1" diameter, 2 m radius of curvature concave mirror on a pyrex substrate and coated with protected gold having a reflectance >95% between 630 nm and 10 μm (Figure 12).[8] The mirror was held in a kinematic mount for easy alignment. The entrance and exit apertures were in the lower left and right corners. Images from mirror A appeared along the top of the mushroom (above the openings), while the images from mirror A' appeared along the "stem" of the mushroom, with the last image falling off the "stem" and exiting the cell.

Mirrors A and A' were two half-moon shaped mirrors constructed using a mirror with the same properties as mirror B and cut along its diameter (Figure 13). These mirrors were

[8]Three sets of White Cell mirrors (consisting of 1 mushroom and 2 half-moons per set) were custom built for the project by Spectrum Thin Films Corp.

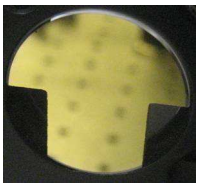

Figure 12: Photograph of "mushroom" mirror used in White Cell

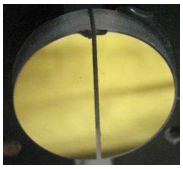

Figure 13: Photograph of "Half-Moon" Mirrors Used in White Cell

attached using epoxy to two planar surfaces of kinematic mounts. The straight edge of the mirrors hung off of each mount slightly so that they could be brought as close together as possible while still allowing free movement of the mounts.

3.3 Cell Conductance

Given that the experiment was designed to look at a "fresh" batch of ions with each pulse, it was necessary to ensure that all of the species from the previous pulse were evacuated from the spectrometer before the next discharge pulse. One way to do this was to look at both the conductance of the cell and the speed of the pump to determine how long, given these conditions, the pump required between pulses to completely evacuate the cell. The calculations follow.

First, at the pressures of hydrogen used in this experiment (1.885 Torr), we fall into the viscous flow region. The equation for conductance for this region is given by Equation 1.

$$C = 32,600 \frac{D^4}{\eta L} P_{av} \text{ L} \cdot \text{s}^{-1} \tag{1}$$

D is the diameter of the tube in cm, η is the viscosity of the gas in micropoise (μ P), L is the length of the tube in cm, and P_{av} is the pressure in Torr.

At an estimate of 100K in temperature (actual temperatures in the LN_2-cooled discharge range from 100 K - 200 K), the viscosity of the gas (after a conversion factor) given in the CRC Handbook of Chemistry and Physics [4] is 42 μP. For water-cooled measurements (temperatures ∼300 K), the CRC lists a viscosity of the gas (after a conversion factor) as 90 μP at 300K. While not incredibly precise, these numbers provided a very reasonable "ball-park" estimate.

Next, we needed to determine the different parts of the system that have different conductances. These are given in Table 1 with an example conductance calculation shown in Equation 2. The individual conductances at 100 K and 300 K are given in Table 2.

Table 1: Dimensions of different parts.

Part	Occurrences	Diameter (cm^{-1})	Length (cm^{-1})
Large Pump Tube	1	7	40
Small Pump Tube	1	1.27	93
Glass End Caps	2	2.54	16
Glass Tube	1	8	160

$$C = 32,600 \times \frac{(1.27\,cm)^4}{42\,\mu P \cdot 84\,cm} \times 3\,Torr = 72\ \mathrm{L \cdot s^{-1}} \tag{2}$$

Next, it was necessary to compute the total conductance of the cell. The equation for total

Table 2: Conductance ($L{\cdot}s^{-1}$) of different parts at 100 K and 300 K and 1.85 Torr.

Part	Occurrences	Conductance (100 K)	Conductance (300 K)
Large Pump Tube	1	87824	40985
Small Pump Tube	1	41	19
Glass End Caps	2	3806	1776
Glass Tube	1	37456	17479

conductance of parts in series (as in our experiment), is given by Equation 3, and the actual calculations are shown in Equations 4 and 5.

$$C_{series} = [\frac{1}{C_1} + \frac{1}{C_2} + \frac{1}{C_3} + ...]^{-1} \tag{3}$$

$$C_{series}(100K) = [\frac{1}{37456} + \frac{2}{3806} + \frac{1}{87824} + \frac{1}{41}]^{-1} \simeq 40\ L \cdot s^{-1} \tag{4}$$

$$C_{series}(300K) = [\frac{1}{17479} + \frac{2}{1776} + \frac{1}{40985} + \frac{1}{19}]^{-1} \simeq 19\ L \cdot s^{-1} \tag{5}$$

Now, with the conductance in place, we can calculate the pumping speed of the system using the conductance and the pumping speed of our pump as shown in Equation 6 and calculated in Equations 7 and 8. S is the delivered pumping speed of the system, S_P is the speed of our pump (8.33 L·s^{-1}), and C is, of course, the conductance.

$$\frac{1}{S} = \frac{1}{S_P} + \frac{1}{C} \tag{6}$$

$$S_{100K} = (\frac{1}{8.33} + \frac{1}{40})^{-1} = 6.89\ L \cdot s^{-1} \tag{7}$$

$$S_{300K} = (\frac{1}{8.33} + \frac{1}{19})^{-1} = 5.79\ L \cdot s^{-1} \tag{8}$$

Now, we want to see how long it would take the pump to evacuate one "pulse" of discharge from the cell. We make the assumption that the pulse fills the entire cell, but not the tubing going to the vacuum pump, and therefore occupies a volume of 8.5 L. This is actually a "worst-case" scenario, as the pulse does not fill the entire cell. Using this assumption,

Equations 9 and 10 show the calculation of how many seconds it takes to evacuate the cell with average pumping speeds of 6.9 L·s^{-1} and 5.8 L·s^{-1}.

$$8.5\ L \times \frac{1\ s}{6.9\ L} = 1.2\ s \tag{9}$$

$$8.5\ L \times \frac{1\ s}{5.8\ L} = 1.5\ s \tag{10}$$

The duration between pulses was designed to give this calculation a very wide margin of error and to account for abnormalities in the system.

3.4 Liquid Nitrogen Flow Rate

Although the flow rate was never experimentally measured, it is interesting to calculate approximately how much liquid nitrogen flow is required to cool the plasma as much as physically possible.

We start by determining how much power is present in the plasma operating at 1000 V and 1250 mA.

$$P = IV \tag{11}$$

$$= (1.25A)(1000V) \tag{12}$$

$$= 1250W = 1250\frac{J}{s} \tag{13}$$

The power represents how much "heat," in joules, needs to be transfered to the N_2 per second for good cooling. The biggest loss of N_2 ocurrs during the phase change from liquid to gas, a process which, according to the CRC, takes 198.8 J for every gram of nitrogen at

its boiling point.

Knowing how much "heat" is available, we can determine how many grams of nitrogen can be boiled off (thus showing how many grams are required to transfer that much heat.)

$$1250\frac{J}{s} \times \frac{1g}{198.8J} = 6.2877\frac{g}{s} \tag{14}$$

This shows how many grams of liquid nitrogen need to be at a point every second to dissipate the heat. Now we need to convert that into a more easily measured flow rate. Grams per second is a flow rate, but it is not simple to measure how many grams are coming out the end of the tube every second. Instead, we can measure the gas flow rate, by looking at the density of the gas at its boiling temperature. While not completely accurate, it should be good enough to provide a "ball-park" estimate.

$$6.2877\frac{g}{s} \times \frac{1L}{4.622g} = 1.36\frac{L}{s} \tag{15}$$

3.5 Technical Issues

Several issues arose throughout the course of the experiment which necessitated changes to the design of the cathode. First, the original design included brass tubes holding two CaF_2 windows at Brewster's angle. The tubes, however, proved to be so thick-walled that the path traced by light passing through them in the White Cell configuration was clipping on the inside of the tube. Steel tubes with 1/16" thick walls were used instead. The CaF_2 windows could not be removed from the brass tubes without breaking, so they were replaced with BaF_2 windows. BaF_2 was chosen only because of availability reasons; differences in transmission between CaF_2 and BaF_2 are minimal at these frequencies.

Second, issues arose surrounding the discharge itself, especially in the area directly between the anode and the cathode. Due to a breakage in the glass shell, the hole on the cathode for the guide tube was no longer directly beneath the anode. As such, the guide tube was situated at an awkward angle. This not only caused stress on the tube, but it also permitted an excessive amount of arcing to occur between the anode and the outside of the cathode. To combat this, a non-conductive Vespel ring was constructed to slip around the anode and the guide tube, effectively preventing arcing outside the tube. Further, the guide tube was modified to incorporate a "kink" in the middle so that it lined up with both the hole and the anode. The combination of these significantly reduced arcing.

Finally, after a period of running the cell, a persistent 50 mTorr leak was discovered that was present only when the cell was being cryogenically cooled. Shortly thereafter, a 2 Torr leak appeared which significantly affected the results of the experiment. The leak began between 30 minutes and about an hour after the start of liquid-nitrogen flow through the cell and was observed numerous times. H_2O efficiently quenches the formation of H_3^+, thus any significant amount of atmosphere in the cell could have a noticeable effect on the intensity of the absorption signal observed. In this case, such a drop in intensity was indeed observed, and data collected whenever the 2 Torr leak developed were unfortunately useless.

This leak was eventually traced to one of the two o-ring seals at the feedthrough end of the cathode. Although the flanges were wrapped in heating tape kept at a medium-high level and a fan was flowing warm, dry air over them, they consistently frosted over due to the extreme temperatures they were exposed to. This is thought to be the cause for the failure of the viton o-rings. A teflon o-ring was obtained in the correct size for the smaller of the two seals and this replaced the old viton ring. Under cryogenic conditions, the seal held for at least 2 hours. It is hoped that silicone o-rings will provide even more temperature-resistance and an upgrade to all of the existing o-rings on the cathode is planned in the near future.

4 Conclusion

A hollow-cathode cell has been constructed that can support a variety of cooling media and optical setups for spectroscopy. This cell has been used in conjuction with a White-type multipass absorption setup to obtain data on the reaction of $H_3^+ + H_2$ at both water-cooled and liquid nitrogen-cooled temperatures. The results have given new insight into both the mechanisms of this reaction and its astrophysical implications.

Part II

Spectroscopy of N_2^*

5 High Resolution Cavity-Ringdown Spectroscopy of the $B^3\Pi_g \rightarrow A^3\Sigma_u^+$ band system of N_2

5.1 Introduction

The first positive band system ($B^3\Pi_g \rightarrow A^3\Sigma_u^+$) of N_2 was first observed by Deslandres in 1902. The greenish-yellow afterglow of active nitrogen was observed by Lewis in 1904[8] and first characterized as due to bands of the first positive system of N_2 by Fowler and Strutt in 1911 [9]. The first rotational analysis, however, was not performed for several decades until Naudé analyzed the 5-2 and 6-3 bands in 1932 [7] and Van der Ziel the 12-7 and 12-8 bands in 1934 [10].

Since then, this system has been the subject of intense investigation. The analysis of the 1-0 band was published in 1951 by Feast [11] and the 1-0, 2-1, and 3-2 bands in 1952 by Carroll. [12] The most exhaustive study of the system to date was that of Dieke and Heath

in 1959 which covered a total of 21 bands [13]. Roux et al. later extended this analysis to the v=12 level of the $B^3\Pi_g$ state and the v=8 level of the $A^3\Sigma_u^+$ state [14].

We have previously reported the construction of a near-infrared continuous-wave cavity ringdown spectrometer which was used in the study of the N_2^+ Meinel system 2-1 band [15]. During the study, a far greater number of lines than assignable to N_2^+ were observed. An analysis of the Deslandres table found in reference [13] showed 5 bands, 2-2, 3-3, 4-4, 7-8, and 8-9, of the first positive band system of N_2 fell within the 10200-10600 cm^{-1} frequency coverage of our external cavity diode laser. We present here our analysis of the 3-3 band and experimentally determined molecular constants for this band.

To our knowledge, this band has not been previously observed, although some information on its parameters is available from the global analysis of Roux et al. [14], which included the 3-0, 3-1, 0-3, 1-3, 2-3, 7-3, and 8-3 bands.

5.2 Experimental Design

The instrumentation has been described in detail elsewhere [15]. Briefly, we employed continuous-wave cavity ringdown spectroscopy (cw-CRDS) to probe the molecular ions created in a N_2/Ar discharge with our spectrometer shown in Fig 14. The diode laser, tunable from 922-985 nm, was passed through a 50/50 beam splitter into signal beam and a reference beam.

The reference beam was split by a second 50/50 beam splitter for relative frequency calibration. One beam was sent into a homemade wavemeter based on a traveling cart Michelson interferometer with picometer resolution [16]. The second reference beam was split once more with part being sent into a multipass Herriott cell filled with 16 mTorr of water vapor for absolute frequency calibration. The remainder of the beam was sent into a spectrum analyzer and etalon finder.

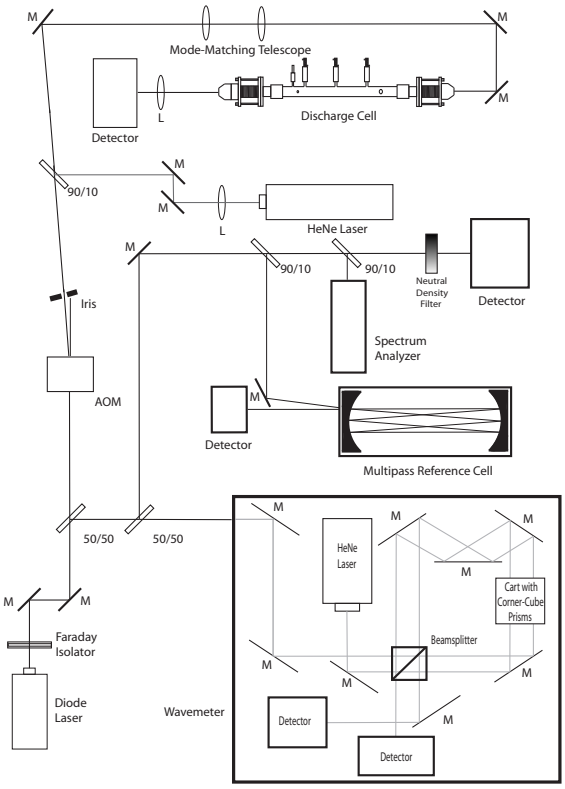

Figure 14: Schematic diagram of the continuous-wave cavity ringdown spectrometer.[15]

The signal beam was passed through an acousto-optic modulator (AOM) and the first-order diffracted beam was then made collinear with the beam from a HeNe laser for alignment. These were passed through a set of mode-matching optics before being coupled into a high-finesse cavity which surrounded the discharge. The discharge itself operated with a current of 70 mA around 3100 V and spectra were recorded at both 3 Torr and 500 mTorr total cell pressure with a constant 300 mTorr background of Argon. The ringdown signals were then collected on an avalanche photo-diode (APD) detector and digitized.

The digitized signals were fit using a LabWindows data acquisition routine and time constants were calculated from this data. The middle 50% of a spread of data collected from 10 ringdowns and 100 reference signals were selected and the average value of the selected points were recorded. Each scan covered ~ 4 cm^{-1} in 1000 steps.

Rough frequency calibration was achieved by referencing the wavemeter. Mode hops were identified through the use of a spectrum analyzer and an etalon finder circuit [15].During a mode-hop-free scan, the etalon finder output appears as a regular sawtooth pattern. A break or discontinuity indicates a mode hop (see Figure 15), but provides no information on how far forwards or backwards in frequency space the laser has shifted. The wavemeter is again referenced in the vicinity of the mode hop and free spectral ranges are added or subtracted from the scan to obtain an excellent relative calibration.

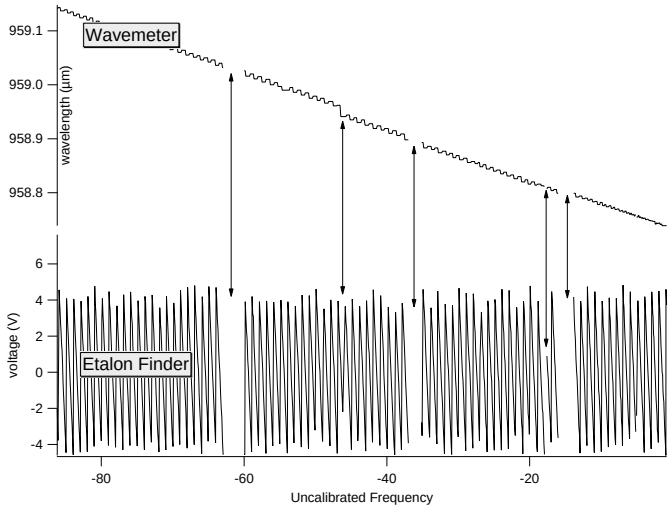

Figure 15: Etalon finder and wavemeter traces. Arrows (↕) show regions where mode hops have occured.

Absolute frequency calibration was achieved by referencing the Herriott cell absorption spectra taken during the scan. Every scan contained at least one water line, with most having two or more. These lines were fit to Gaussians and their center frequencies were assigned to those obtained from the HITRAN database. Using this method, an average fit had a 1 σ uncertainty of $\sim$0.004 cm^{-1}. Fully calibrated cw-CRDS and water spectra and wavemeter and etalon finder traces are shown in Fig 16 for a single scan.

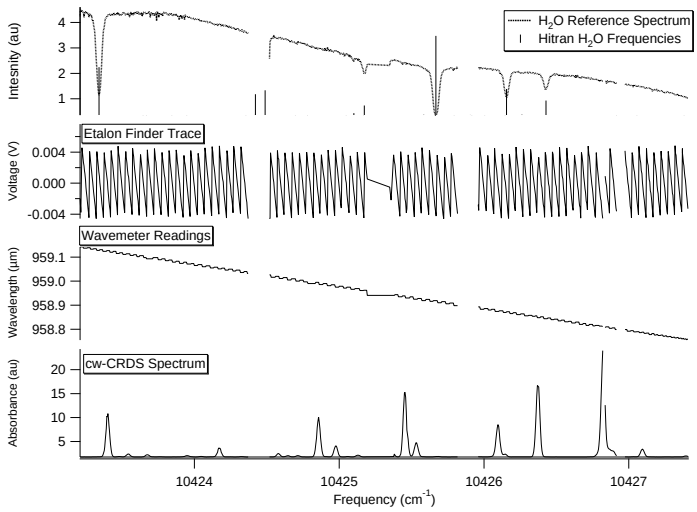

Figure 16: Example calibrated spectrum from $\sim 10423 - 10428$ cm^{-1} showing the cw-CRDS spectrum, reference cell spectrum, and etalon finder and wavemeter traces.

Lines from the 2-1 Meinel system of N_2^+ are present in the frequency range covered, necessitating an approach to differentiate between N_2^+ and N_2* features. To accomplish this, the spectra were collected twice in each frequency window; once at 3 Torr and once at 500 mTorr. N_2* is collisionally quenched at higher pressures, and thus these lines are more intense at 500 mTorr than at 3 Torr. Conversely, N_2^+ is not affected by collisional quenching and thus these lines are stronger at the higher pressures as shown in Fig 17.

Using this method of differentiation, 125 N_2^+ lines were identified and assigned [15] and $\sim$450 N_2* lines were identified.

5.3 Theory

The first positive system of N_2 consists of transitions between the $B^3\Pi_g$ and $A^3\Sigma_u^+$ electronic states. Initial spectral predictions were performed using the program PGOPHER [17]. Spectral parameters for these predictions were either taken directly from those determined by Roux

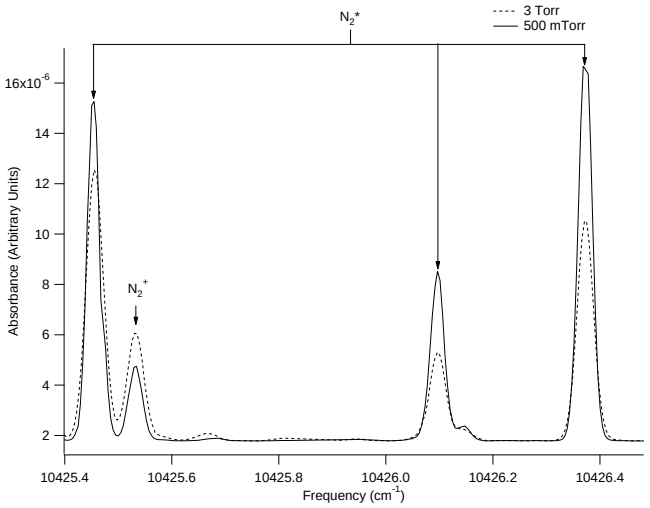

Figure 17: Spectra at 500 mTorr and 3 Torr showing the differences in line intensities for N_2^+ and N_2*.

et al. or calculated from them [14]. The predicted spectrum for the 3-3 band of N_2* at 750 K is shown in Fig 18.

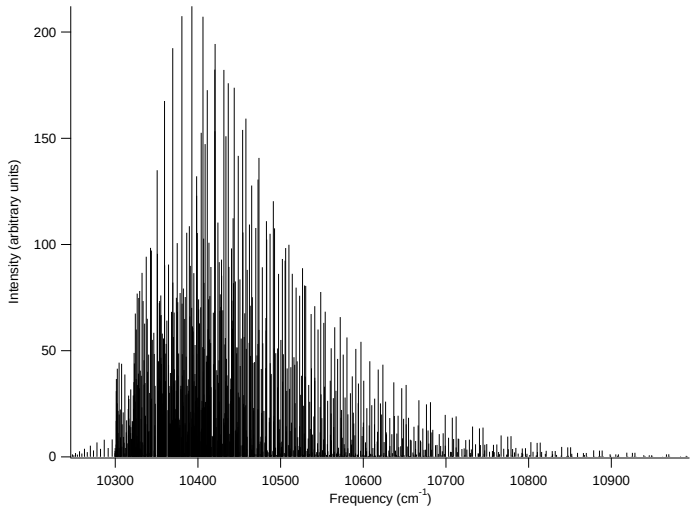

Figure 18: Stick spectrum of N_2 lines predicted by PGOPHER.

The ground $A^3\Sigma_u^+$ state follows Hund's case (b) having spin components $F_1 \Rightarrow J = N + \frac{1}{2}$ and $F_2 \Rightarrow J = N - \frac{1}{2}$. The effective Hamiltonian used contained constants for the band

origin, the rotational constant ($B_{v''}$), the spin-spin coupling constant ($\lambda_{v''}$), the spin-rotation coupling constant (γ) and the quartic centrifugal distortion constant ($D_{v''}$). The value of $\lambda_{v''}$ is equal to 1.5 times the parameter ε used by Roux et al [14].

The excited $B^3\Pi_g$ state follows Hund's case (a) for low values of J, and an intermediate between Hund's cases (a) and (b) at higher values of J. Molecular parameters used were the rotational constant ($B_{v'}$), the spin-orbit coupling constant (A), the spin-spin coupling constant ($\lambda_{v'}$), the spin-spin coupling constant (o) giving Λ doubling, the Λ doubling constants (p and q), and the quartic centrifugal distortion constant ($D_{v'}$). The value of o is related to that of α given in in Roux et al. [14] by $\alpha = o + p + q$.

5.4 Results and Discussion

Analysis of this system is on-going. There appears to be a discrepency in the Hamiltonians used by PGOPHER and Roux et al [14]. This has unfortunately led to great difficulty in simulating the transitions of interest, and thus in assigning the experimental spectrum. Futher, until this difference is resolved, comparison between experimentally determined constants and the literature values is impossible.

5.5 Conclusion

Work has been completed on the assignment of high-resolution spectra of N_2^* collected using cavity-ringdown spectroscopy. Spectra have been collected and well calibrated. Final assignment of the transitions can be completed once discrepencies between PGOPHER and the literature are resolved.

6 Appendix A - Calibration Routine

6.1 Introduction

A routine for calibrating spectra obtained from the N_2 experiment was developed by Michael Wiczer in the program Igor. The basic steps for calibrating a spectra is described here. These steps were derived in large part from the notebook of Bogdan Negru with annotations by Susanna Widicus Weaver.

6.2 Loading a Scan

1. Open the Igor Experiment containing the calibration routine.
2. Load a scan file (Data → Load Waves → Load General Text)
3. Load the necessary columns, delete all others. Necessary Columns are:
   (a) voltage
   (b) reference (input 4)
   (c) wavemeter (input 6)
   (d) spectrum
   (e) etalon (input 0)

6.3 Rough Calibration

First, the etalon file needs to be fixed. Panel 5 (Figure 19) is designed to do this. Select the etalon file just loaded from the drop down menu and append "fixed" to the end of it in the box below. Then run the panel.

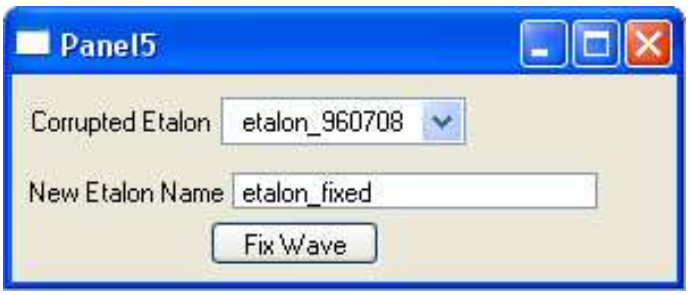

Figure 19: Panel 5 - Fixing the Etalon File

Next, a new x-wave needs to be generated. Panel 2 (Figure 20) is designed to do this. This panel requires inputs for the spectrum and wavemeter waves that were loaded, as well as the **fixed** etalon wave. Rename the x-wave to something descriptive. The mod-hop sensitivity should be left at 0.75. This will generate a new x-wave that is later turned into a frequency-calibrated wave and also fixes glaringly obvious mode hops.

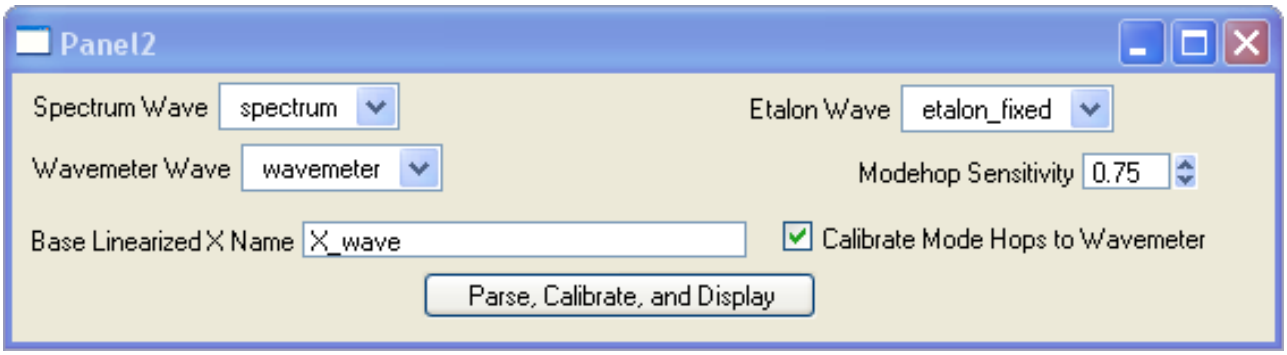

Figure 20: Panel 2 - Creating an X-Wave

After this, graph the wavemeter wave versus the new x-wave. Figure 21 is provided for reference to this discussion. The "stepping" of the trace is normal due to the physical function of the wavemeter. Problem areas occur when either the wavemeter stopped reading, or there was a mode hop. If the wavemeter stopped reading, this is evidenced by a discontinuity in the actual trace. These can be large vertical, horizontal, or angular jumps. These can be identified by placing the cursors at the beginning of a jump and stepping it across one point

at a time. If the cursor registers a large jump (i.e. the entire chunk of suspect line has no intermediate points), then the wavemeter stopped reading there and it needs to be fixed. The other type of issue is mode hops between chunks of trace. If a scan has been completely corrected for mode hops, the chunks will align linearly. The simplest way to identify these is to search by eye, and then align the edge of a piece of paper along the top of a trace. If the next chunk falls above or below the edge of the paper, it needs to be fixed.

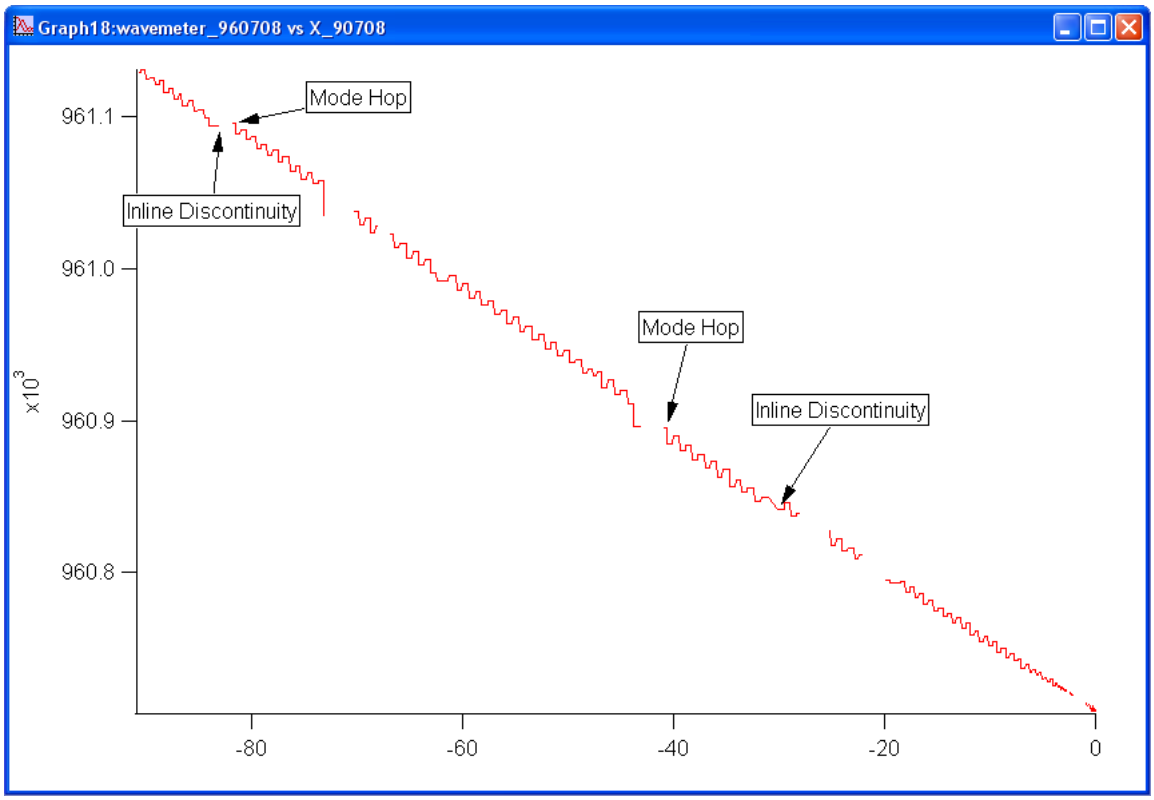

Figure 21: Wavemeter vs x-wave

To correct these issues, manually add and subtract free spectral ranges (FSRs) from the scan. A command has been built into Igor for just this purpose. First, locate the exact beginning or end of the area using the cursors. Then, you can add or subtract the FSRs using the following command:

```
addFSRs('xwave',point\#,FSR,1)
```

To add a FSR, insert a positive number for "FSR" (i.e. 1, 2, or 3 adds 1, 2, or 3 FSRs, respectively). To subtract a FSR, simply add a negative sign in front. Do this until all discontinuities are resolved (as best as reasonably possible) and until the chunks of trace align linearly (this is an absolute must).

If the scan is very close to linear, a command exists to double check the rough calibration. This command is fairly safe, but can occasionally cause issues in more complicated situations, so use it judiciously.

```
doubleCheckMH(xwave,wavemeter,FSR)
```

Finally, the x-wave needs to be scaled so that a FSR is 0.05. Do this by executing the command:

```
 'xwave'*=0.05
```

.

6.4 Absolute Calibration

The wavemeter should provide a rough idea of where the scan starts and stops. Using this knowledge, pull up an appropriate chunk of the water lines from HITRAN. Next, pull up a graph of the reference spectrum versus the x-wave. Using relative positions and intensities, determine the water lines present in the scan. A scan must have at least one water line to be even remotely well calibrated. To be really confident, a scan should have three lines, one at each end and one in the middle of the scan. A group of lines clumped together at one end or the other produces a less reliable scan.

Once the lines have been identified, make note of the exact frequencies from the HITRAN line list. Next, the exact location of the lines in the reference scan need to be identified. The top half of Panel 3 (Figure 22) is designed to do this.

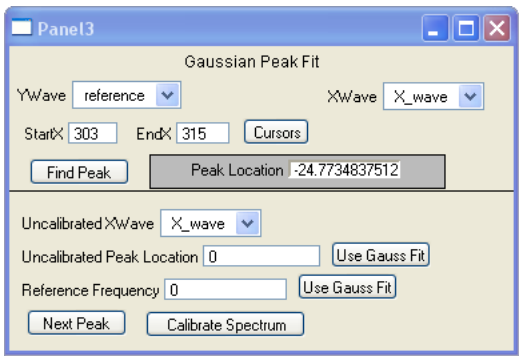

Figure 22: Panel 3: Absolute Calibration

Select your reference and x-waves from the drop down menus. Next, place the cursors at the left and right of the line in question, as close to the base as possible. Click the "cursors" button to load the locations of the cursors into the panel. Click "find peak." This will do a gaussian fit to the region between the cursors and locate the peak of the line.

Next, move to the bottom of the panel and again select the x-wave from the drop down list. Click the "Use Gauss Fit" button next to the "Uncalibrated Peak Location" field to fill the field in using the peak location calculated in the top half. Manually enter the frequency obtained for the peak from HITRAN in the "Reference Frequency" field. Click the "Next Peak" button.

IMPORTANT! The "Next Peak" button must always be pressed before the "Calibrate Spectrum" button, even if there is only one peak to calibrate.

Repeat this process for each water line in the reference scan. When all have been entered, click the "Calibrate Spectrum" button. Congratulations! The scan is now calibrated!

6.5 Validating

One way to double check the accuracy of the calibration is to compare the calibrated spectra from the same region. There should be almost no difference between the calibrated peak locations in the two scans.

References

[1] M. Cordonnier et al., *J Chem Phys* **2000**, *113*, 3181.

[2] B. A. Tom, M. Wiczer, A. A. Mills, K. N. Crabtree, and B. J. McCall, *JCP* **2009**, *In Preparation.*

[3] J. U. White, *J. Opt. Soc. Am.* **1942**, *32*, 285-288.

[4] CRC Handbook of Chemistry and Physics. http://www.hbcpnetbase.com

[5] B. A. Tom, S. Bhasker, Y. Miyamoto, T. Momose, B. J. McCall, *Rev. Sci. Inst.* **2009**, *80*, 016108

[6] B. A. Tom, B. A. McGuire, N. Indriolo, M.B. Wiczer, L. E. Moore, T. J. Wood, and B. J. McCall, *In Preparation.*

[7] S. M. Naudé, *Proc. Roy. Soc.* **1932**, *136*, 114-144.

[8] P. Lewis, *Astrophys. J.* **1904**, *20*, 49-58.

[9] A Fowler and R. J. Strutt, *Proc. Roy. Soc. London A.* **1911**, *85*, 377-388.

[10] A. Van der Ziel, *Physica* **1934**, *1*, 353-362.

[11] M. W. Feast, *Proc. Phys. Soc. London A* **1951**, *63*, 568-574.

[12] P. K. Carroll, *Proc. Roy. Irish. Acad. A* **1952**, *54*, 369-397.

[13] G. H. Dieke and D. F. Heath, Johns Hopkins Spectroscopic Report Number 17, **1959**.

[14] F. Roux, F. Michaud, and J. Verges, *J. Mol. Spec.* **1983**, *97*, 253-265.

[15] S. L. Widicus Weaver et al, *J. Mol. Spec.* **2008**, *249*, 14-22.

[16] J. P. DiGangi, B.S. Thesis, University of Illinois at Urbana-Champaign, http://bjm.scs.uiuc.edu/pubs/DiGangi_thesis.pdf, **2006**.

[17] PGOPHER, a Program for Simulating Rotational Structure, C. M. Western, University of Bristol, http://pgopher.chm.bris.ac.uk